A novel SVPWM control algorithm for switching power amplifier of active magnetic bearings

Shiwen Li, Zhiquan Deng*, Kexiang Li, Jiaxi He
College of Automation Engineering, Nanjing University of Aeronautics and Astronautics, China
*E-mail: dzq@nuaa.edu.cn

Abstract — Space vector pulse width modulation (SVPWM) control algorithm is commonly used for power electronic converters. This control method can be applied to two-phase three-leg switching power amplifier for two degree-of-freedom (DOF) control coils, reducing the number of switching tubes and increasing the power density of the control systems. The reference voltage of SVPWM is usually calculated by PID controller. However, the PID parameters are difficult to adjust, and there will be chaos phenomenon. A new control method was proposed in this paper. Digital one-cycle control algorithm was used to calculate the reference voltage for SVPWM, which has the advantages of simple structure, high control accuracy, rapid response and no overshoot. Besides, In order to improve the control accuracy, a one-cycle algorithm model was established considering the resistance of magnetic bearing coil. Simulation proves that with this control strategy, the current closed-loop control has an ideal performance.

I. INTRODUCTION

As a high-performance novel bearing, the magnetic bearing has no contact with the rotor, no lubrication, no mechanical friction, and can be actively controlled. And due to these characteristics, it can be applied to extreme situations such as vacuum, clean space, high temperature, and strong corrosiveness[1]. In fact, magnetic bearings have a wide range of applications in energy storage flywheels, turbomachinery, high-speed spindles and other occasions.

Active magnetic bearings take control of rotor position by controlling levitation forces. The levitation force is linear with the control current. Therefore, to achieve accurate control of the levitation force, it is very important to investigate the current inner loop control algorithm with good control performance.

Current inner loop control algorithms currently used can be mainly divided into two major categories: current mode control and voltage mode control. The current mode control includes current hysteresis control, sample-hold, minimum pulse width modulation and other control strategies. This type of control strategies is more suitable for analog control. The voltage mode control usually uses pulse width modulation, which can be divided into PID control and one-cycle control according to the difference of the pre-controller. Besides, according to the method of pulse width modulation, it can be divided into PWM, SPWM, SVPWM, etc[2].

SVPWM can be applied to three-leg main circuit topology. When applied to a power amplifier of magnetic bearings, it can drive two degrees of freedom coils at the same time, reducing the number of switching tubes, thereby reducing the volume of the power amplifier, reducing the cost, and improving the power density[3][5]. At present, switching power amplifiers controlled by SVPWM usually use PID controllers as the pre-controller[6]. This control strategy is simple and easy to implement. However, it has some disadvantages such as difficulty of optimal parameter design, conflict between tracking speed and overshoot, and poor tracking accuracy.

One-cycle control is usually used in analog control, and the application of one-cycle analog control is generally voltage switching power amplifier. The literature [7], [8] (PFC converters), [9] (three-phase three-level VIENNA rectifiers), [10], [11] (dual-input Buck converters) studies the one-cycle control of analog amplifiers. The literature [12] proposed the method of digital one-cycle control. The literature [13] proposed a one-cycle algorithm applied to the main circuit topology of multi-bridge arm. In these literatures, digital one-cycle cotrol algorithm use PWM modulation.

In this paper, one-cycle control is used as pre-controller of SVPWM, which can accurately calculate the reference voltage for each switching cycle[12]. Switching power amplifiers with this control strategy have fast response, high tracking accuracy, and no overshoot, while retaining the advantages of SVPWM for a three-leg main circuit.

II. MAIN CIRCUIT TOPOLOGY

The novel switching amplifier studied in this paper is applied to permanent magnetic bias bearings. Therefore, the amplifiers are required to provide bidirectional current. Based on the above considerations, this paper uses the two-phase three-leg main circuit topology, as shown in Figure 1.

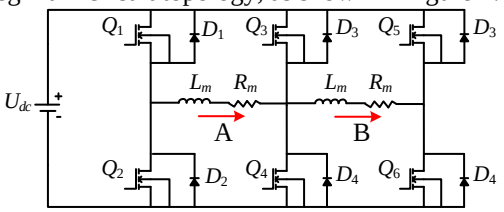

Fig. 1. Main circuit topology for SVPWM switching amplifier

The circuit uses six MOSFETs to form three bridge arms that drive 2 DOF control coils. The Q_3 and Q_4 bridge arm is common bridge arm. Since two switching tubes of the same bridge arm cannot be turned on at the same time, the switching state of each bridge arm can be represented by S_1, S_2, and S_3. 1 indicates that the upper mosfet is opened and the lower mosfet is turned off, and 0 indicates that the upper tube is turned off and the lower tube is opened. Then there are eight switching states for the entire switching power amplifier and eight basic voltage vectors are generated. As shown in Table 1.

Table 1 Basic voltage vectors

Voltage Vector	S_1	S_2	S_3	U_A	U_B
U_0	0	0	0	0	0
U_1	0	0	1	0	$-U_{dc}$
U_2	0	1	0	$-U_{dc}$	U_{dc}
U_3	0	1	1	$-U_{dc}$	0
U_4	1	0	0	U_{dc}	0
U_5	1	0	1	U_{dc}	$-U_{dc}$
U_6	1	1	0	0	U_{dc}
U_7	1	1	1	0	0

It can be seen that under the three-leg main circuit topology, 2 DOF control coils share two switching tubes. As a result, the number of switching tubes can be reduced, the

volume of power amplifier is smaller, the cost is lower, and the power density is higher. The 2 DOF control coils have three voltage states U_{dc}, - U_{dc} and 0, indicating that this switching power amplifier can perform three-level modulation with the advantage of low current ripple.

III. Implementation of One-cycle Control Based on SVPWM

Block diagram of current closed-loop control algorithm for magnetic suspension bearing is shown in Figure 2. In this figure, i_{Aref} and i_{Bref} are the given currents of 2 DOF respectively, i_{Afed} and i_{Bfed} are the feedback currents of 2 DOF respectively, L is the inductance value of control coils, R is the resistance value of control coils, T_s is the switching period, u_{Aref} and u_{Bref} are respectively reference voltages for 2 DOF. The given current is calculated by the displacement closed-loop controller according to the displacement of the rotor. The actual current is measured by the current sensor. The one-cycle controller calculates the given voltage in one cycle according to the given current and the actual current. The SVPWM module generates control signals for switching tubes to generate the given voltages of 2 DOF respectively, so that the actual current can be tracked in each cycle.

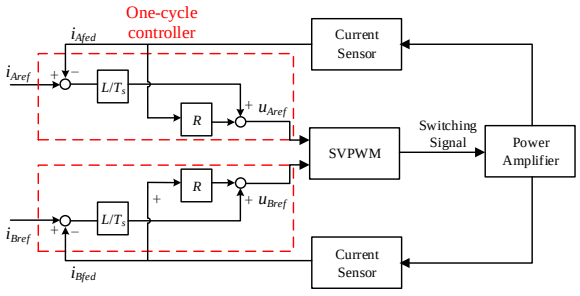

Fig. 2. Block diagram of closed-loop control algorithm

3.1 *Modeling of One-cycle Control Algorithm*

The main idea of one-cycle control algorithm in this paper is to accurately calculate the reference voltage required for each cycle, so that the amount of current change in each cycle is strictly equal to the control amount.

Taking the control coil of A DOF as an example, assuming that the voltage across the coil is U, the expression of the voltage U can be listed as:

$$U = L\frac{di}{dt} + iR \tag{1}$$

where L is the inductance of the control coil, R is the resistance of the control coil, and i is the current in the coil.

The equation of state of i can be listed by the above expression as:

$$\frac{U}{s} = LsI(s) - Li(t_0) + RI(s) \tag{2}$$

The time domain expression of coil current i can be solved as:

$$i(t) = \frac{U}{R}\left(1 - e^{-\frac{R}{L}(t-t_0)}\right) + i(t_0)e^{-\frac{R}{L}(t-t_0)} \tag{3}$$

Since the value of $R(t-t_0)/L$ is very small, it can be considered that:

$$\lim_{\frac{R}{L}(t-t_0)\to 0}\left(1 - e^{-\frac{R}{L}(t-t_0)}\right) = 0 \tag{4}$$

Then, within one switching period of t_0 to t_0+T_s, the amount of current change is:

$$\Delta i = \frac{T_s}{L}\left(U - i(t_0)R\right) \tag{5}$$

The final value is tracked as the target of control, that is, at the end of each switching cycle, the given current can be tracked by the actual current. Then, the expression of the amount of current change in one cycle is:

$$\Delta i = i_{ref} - i(t_0) \tag{6}$$

According to (5) and (6), voltage value across the coil required to produce the corresponding current change can be solved

$$U_{ref} = \frac{L\left(i_{ref} - i(t_0)\right)}{T_s} + i(t_0)R \tag{7}$$

The one-cycle controller calculates the voltage value as a reference voltage and outputs it to the SVPWM module.

3.2 Phase Compensation for One-cycle Control

In one-cycle control, since the control target at the beginning of the cycle is realized at the end of the cycle, there is an inevitable delay of the control system[14]. As a result, the actual current always lags behind the given current by a certain phase. The phase delay of actual current will affect performance of the switching power amplifier, and even affect its stability. Therefore, the phase lag caused by control is compensated in this paper.

Under digital one-cycle control, delay of control system of switching power amplifier mainly consists of the following components: Delay T_{ad} caused by AD conversion which is mainly related to the sample rate of AD sampling chip. Delay T_{cal} caused by calculation which mainly depends on the complexity of the algorithm and the calculation waiting time. Delay T_c caused by the control algorithm. Under digital one-cycle control algorithm, T_c=T_s is used when the final value is tracked, and T_c=T_s/2 is used when the mean value is tracked. And delay of circuit T_e. Relative to several other time constants, T_e is small and can be ignored.

In summary, the total delay of control system is

$$T_d = T_{ad} + T_{cal} + T_c \tag{8}$$

Multiply the previous system's transfer function by an advanced link to compensate for the system for T_d

$$\Phi_{comp}(s) = \Phi(s)e^{sT_d} \tag{9}$$

The transfer function block diagram of the compensated control system is shown in Figure 3, where I_{ref}(s) is the reference current given by the outer loop of control system for magnetic bearing, I_{ad}(s) is the given current after AD sampling, I_{comp}(s) is the given current after compensation, I(s) is the output current of the switching amplifier.

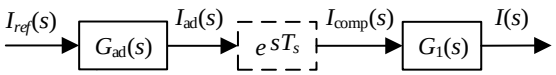

Fig. 3. Block diagram of the compensated control system

The Fourier expansion of the advance link e^{sTd} and the delay

links e^{-sTs} and e^{-2sTs}:

$$\begin{aligned} e^{sT_d} &= 1+sT_d+\frac{1}{2!}(sT_d)^2+\cdots \\ e^{-sT_s} &= 1-sT_s+\frac{1}{2!}(sT_s)^2+\cdots \\ e^{-2sT_s} &= 1-2sT_s+\frac{1}{2!}(2sT_s)^2+\cdots \end{aligned} \tag{10}$$

Write e^{sTd} as an expression for e^{-sTs} and e^{-2sTs}:

$$e^{sT_d} = x_0 + x_1 e^{-sT_d} + x_2 e^{-2sT_d} \tag{11}$$

Then

$$\begin{aligned} x_0 + x_1 + x_2 &= 1 \\ -x_1 - 2x_2 &= \frac{T_d}{T_s} \\ x_1 + 4x_2 &= \left(\frac{T_d}{T_s}\right)^2 \end{aligned} \tag{12}$$

Convert expressions to matrices:

$$\mathbf{A}=\begin{pmatrix} 1 & 1 & 1 \\ 0 & -1 & -2 \\ 0 & 1 & 4 \end{pmatrix}, \mathbf{x}=\begin{pmatrix} x_0 \\ x_1 \\ x_2 \end{pmatrix}, \mathbf{y}=\begin{pmatrix} 1 \\ \frac{T_d}{T_s} \\ \left(\frac{T_d}{T_s}\right)^2 \end{pmatrix} \tag{13}$$

The value of **x** can be solved as:

$$\mathbf{x}=\mathbf{A}^{-1}\mathbf{y}=\begin{pmatrix} \frac{T_s^2+1.5T_sT_d+T_d^2}{T_s^2} \\ \frac{-2T_sT_d-T_d^2}{T_s^2} \\ \frac{0.5T_sT_d+0.5T_d^2}{T_s^2} \end{pmatrix} \tag{14}$$

This gives the compensation model:

$$\begin{aligned} e^{-sT_d} &= \frac{T_s^2+1.5T_sT_d+T_d^2}{T_s^2}+\frac{-2T_sT_d-T_d^2}{T_s^2}e^{-sT_s} \\ &+\frac{0.5T_sT_d+0.5T_d^2}{T_s^2}e^{-2sT_s} \end{aligned} \tag{15}$$

Block diagram of compensation model is shown in Figure 4.

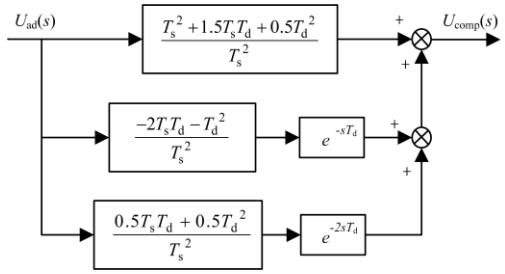

Fig. 4. Block diagram of closed-loop control algorithm

It can be considered in the system that:

$$T_d \approx T_c = T_s \tag{16}$$

The compensation model for phase delay can therefore be simplified to:

$$U_{comp}(s) = 3U_{ad}(s) - 3U_{ad}(s-T_s) + U_{ad}(s-2T_s)s \tag{17}$$

3.3 *Implementation of SVPWM*

Taking the direction of the voltage vector $\boldsymbol{u}_A$ on the A degree-of-freedom (DOF) coil as the direction of x-axis and the direction of the voltage vector $\boldsymbol{u}_B$ on the B DOF coil as the direction of y-axis, then a plane coordinate system can be established. Eight basic voltage vectors divide the plane into six sectors. The spatial distribution of the basic voltage vectors is shown in Fig. 5.

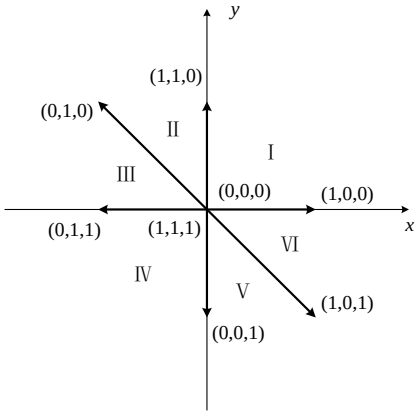

Fig. 5. Spatial distribution of basic voltage vectors

The realization of SVPWM is divided into three steps: selecting the sector, calculating the basic voltage vector action time, determining the basic voltage vector sequence, and finally determining the switch signal[15][17].

A. Selection of Sector

The space voltage vectors in the magnetic bearing is different from the space voltage vectors of the three-phase winding voltage in the motor. It is composed of the voltages of two control coils and therefore is not uniformly distributed in space, as shown in Figure 2. Define the angle between the voltage vector and x-axis as θ. Eight basic voltage vectors divide the space into the following six sectors.

(1) $0 \le \theta < \frac{\pi}{2}$; (2) $\frac{\pi}{2} \le \theta < \frac{3\pi}{4}$; (3) $\frac{3\pi}{4} \le \theta < \pi$; (4) $\pi \le \theta < \frac{3\pi}{2}$;

(4) $\frac{3\pi}{2} \le \theta < \frac{7\pi}{4}$; (5) $\frac{7\pi}{4} \le \theta < 2\pi$

Based on the angle between the reference voltage vector and x-axis, it can be judged which sector the vector is in, thereby determining two basic voltage vectors adjacent to it.

B. Calculation of the Effect Time of Basic Voltage Vectors

Pre-stage one-cycle controller calculates the reference voltage vector $\boldsymbol{u}_{ref}$ with a fixed period T_s. Assume that the two adjacent vectors of the reference voltage vector $\boldsymbol{u}_{ref}$ are $\boldsymbol{u}_1$ and $\boldsymbol{u}_2$., and the action time is t_1 and t_2, respectively. Assuming the effect time of zero vector is t_0, the reference voltage can be expressed as:

$$\boldsymbol{u}_{ref} = \frac{\boldsymbol{u}_1 t_1 + \boldsymbol{u}_2 t_2}{T_s} \tag{18}$$

The effect time of zero vector is:

$$t_0 = T_s - t_1 - t_2 \tag{19}$$

Write equation (18) in a matrix as:

$$\boldsymbol{u}_{ref} = \frac{1}{T_s}\begin{bmatrix} t_1 & t_2 \end{bmatrix}\begin{bmatrix} \boldsymbol{u}_1 \\ \boldsymbol{u}_2 \end{bmatrix} \tag{20}$$

Effect time of two basic voltage vectors can be solved:

$$\begin{bmatrix} t_1 & t_2 \end{bmatrix} = \boldsymbol{u}_{ref} T_s \begin{bmatrix} \boldsymbol{u}_1 \\ \boldsymbol{u}_2 \end{bmatrix}^{-1} \tag{21}$$

Equation (21) can be used to find the effect time of basic voltage vectors for each of the six sectors. The time of basic voltage vectors of six sectors is as follows:

$$[t_1 \quad t_2] = \begin{cases} \begin{bmatrix} \frac{|\boldsymbol{u}_{ref}|T_s\cos\theta}{U_{dc}} & \frac{|\boldsymbol{u}_{ref}|T_s\sin\theta}{U_{dc}} \end{bmatrix} & N=1 \\ \begin{bmatrix} -\frac{|\boldsymbol{u}_{ref}|T_s\cos\theta}{U_{dc}} & \frac{|\boldsymbol{u}_{ref}|T_s(\sin\theta+\cos\theta)}{U_{dc}} \end{bmatrix} & N=2 \\ \begin{bmatrix} \frac{|\boldsymbol{u}_{ref}|T_s\sin\theta}{U_{dc}} & -\frac{|\boldsymbol{u}_{ref}|T_s(\sin\theta+\cos\theta)}{U_{dc}} \end{bmatrix} & N=3 \\ \begin{bmatrix} -\frac{|\boldsymbol{u}_{ref}|T_s\sin\theta}{U_{dc}} & -\frac{|\boldsymbol{u}_{ref}|T_s\cos\theta}{U_{dc}} \end{bmatrix} & N=4 \\ \begin{bmatrix} -\frac{|\boldsymbol{u}_{ref}|T_s(\sin\theta+\cos\theta)}{U_{dc}} & \frac{|\boldsymbol{u}_{ref}|T_s\cos\theta}{U_{dc}} \end{bmatrix} & N=5 \\ \begin{bmatrix} \frac{|\boldsymbol{u}_{ref}|T_s(\sin\theta+\cos\theta)}{U_{dc}} & -\frac{|\boldsymbol{u}_{ref}|T_s\sin\theta}{U_{dc}} \end{bmatrix} & N=6 \end{cases} \tag{22}$$

C. *Determination of the Order of Basic Voltage Vectors*

According to different implementation methods, SVPWM can be divided into 5-segments method and 7-segments method. The zero vector in the 5-segment method is placed in the middle of a switching cycle. In the 7-segment method, the zero vector is divided into four equal parts, one for the beginning and end of a switching cycle, and two for the middle of a switching cycle. Distribution of the switching states is symmetrical, the harmonic content of the output waveform is small, and a reasonable arrangement of the vector action sequence ensures that only one bridge arm operates between each two switching states. In this paper, 7-segment method SVPWM is used. The specific implementation is shown in Table 2, where N is the sector number.

Table 2 Order of the basic voltage vectors

N	$\frac{1}{4}t_0$	$\frac{1}{2}t_1$	$\frac{1}{2}t_2$	$\frac{1}{2}t_0$	$\frac{1}{2}t_2$	$\frac{1}{2}t_1$	$\frac{1}{4}t_0$
1	(0,0,0)	(1,0,0)	(1,1,0)	(1,1,1)	(1,1,0)	(1,0,0)	(0,0,0)
2	(0,0,0)	(0,1,0)	(1,1,0)	(1,1,1)	(1,1,0)	(0,1,0)	(0,0,0)
3	(0,0,0)	(0,1,0)	(0,1,1)	(1,1,1)	(0,1,1)	(0,1,0)	(0,0,0)
4	(0,0,0)	(0,0,1)	(0,1,1)	(1,1,1)	(0,1,1)	(0,0,1)	(0,0,0)
5	(0,0,0)	(0,0,1)	(1,0,1)	(1,1,1)	(1,0,1)	(0,0,1)	(0,0,0)
6	(0,0,0)	(1,0,0)	(1,0,1)	(1,1,1)	(1,0,1)	(1,0,0)	(0,0,0)

From this, the operating time of each bridge arm can be determined. Taking the first sector as an example, opening times of the upper tube of the three bridge arms are respectively as follows:

$$T_{sw1} = \frac{1}{4}t_0$$

$$T_{sw2} = \frac{1}{4}t_0 + \frac{1}{2}t_1$$

$$T_{sw2} = \frac{1}{4}t_0 + \frac{1}{2}t_1 + \frac{1}{2}t_2$$

IV. SIMULATION VERIFICATION

In the simulink environment of MATLAB, the SVPWM controlled switching power amplifier of magnetic bearing was simulated. The sampling frequency of the system was 450 kHz and control frequency of one-cycle was 50 kHz. SVPWM used a 7-segment symmetric method and is implemented by m-language programming. The simulation conditions are as follows: DC bus voltage was 50V, coil inductance was 3.5mH, coil resistance was 2Ω, and MOSFET were used as power component.

Figure 6 shows the waveforms of three bridge arms' switching signals when the reference voltage vector falls in the first sector. It can be seen that under the 7-segment method SVPWM control, in a switching cycle, the distribution of switching state is symmetrical. Three bridge arms' switching states are all changed twice and only one bridge arm operates at a time.

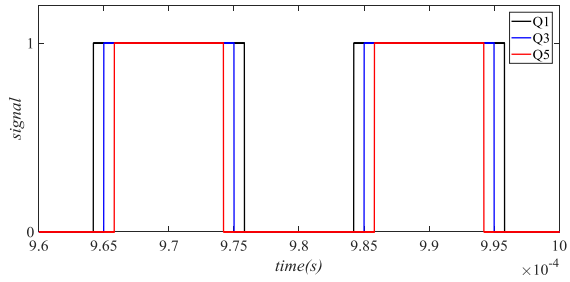

Fig. 6. Waveforms of three bridge arms' switching signals

Figure 7 shows the waveforms of two given current signals of switching power amplifier and two output current signals of control coils. Input signal 1 is a square wave signal with an amplitude of 2A and a frequency of 500 Hz as shown in Fig6(a). Input signal 2 is a sine signal with an amplitude of 2 A and a frequency of 500 Hz as shown in Fig6(c). Figure 8 shows the SVPWM waveforms of three legs' upper tubes under the given signal.

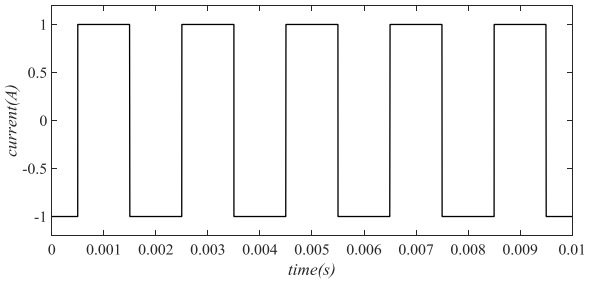

(a) Waveform of given square wave signal

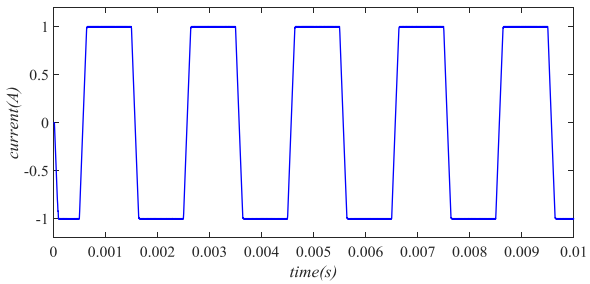

(b) Waveform of actual square wave signal

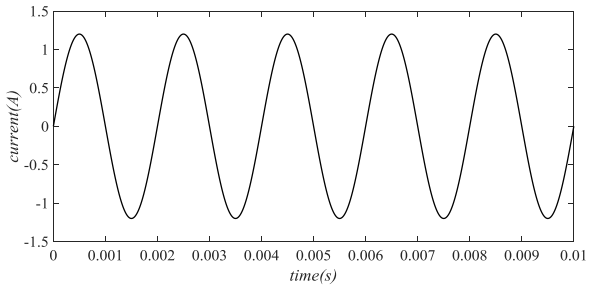

(c) Waveform of given sine wave signal

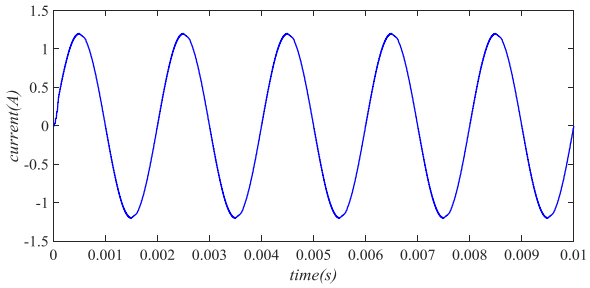

(d) Waveform of actual sine wave signal

Fig. 7. Waveforms of current tracking under the novel SVPWM control algorithm

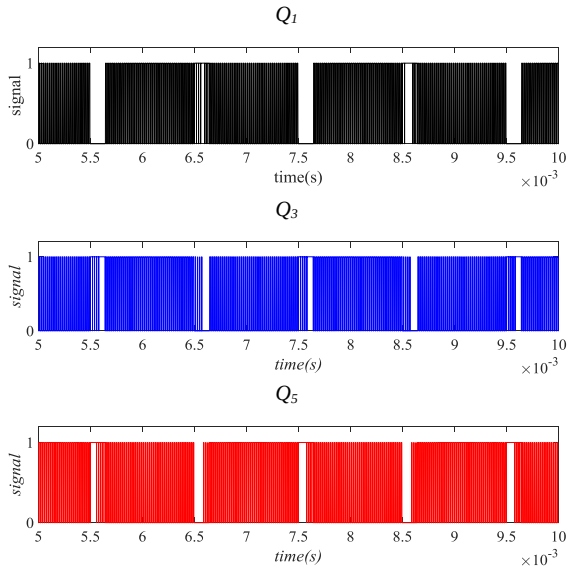

Fig. 8. Waveforms of three bridge arms' switching signals

From the simulation results, it can be seen that under the premise that the 2 DOF control coils share one bridge arm, the one-cycle control SVPWM switching power amplifier can still independently control current in the 2 DOF coils. The actual current of 2 DOF can track the given current very well. The response speed is fast, the current ripple is small, there is no overshoot, and the tracking effect is good.

Under the premise that the given signal of B DOF is zero, conventional PID controller and one-cycle controller were respectively used as the pre-controller to track the step signal with an amplitude of 1.2A given by A DOF.

Select two different sets of PID parameters, the waveforms of current under the three algorithms are shown in Figure 9.

The first set of PID parameters: Kp=250, Ki=2e4, and Kd=4e-4, tracking speeds of PID control and one-cycle control are basically the same, but under PID control, the actual current has obvious overshoot, and there is a steady-state error. There is no overshoot and almost no steady-state error in one-cycle control.

The second group of PID parameters: Kp=100, Ki=3e4, and Kd=4e-4, There is no overshoot both under PID control and one-cycle control, but under PID control, the tracking speed is significantly slower than that under one-cycle control.

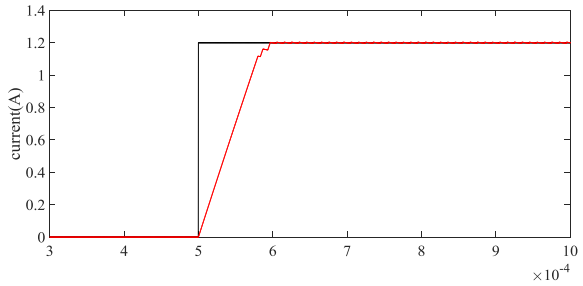

(a) Waveform under one-cycle control

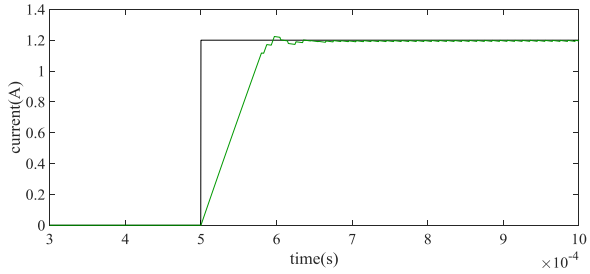

(b) Waveform under first set of PID parameters

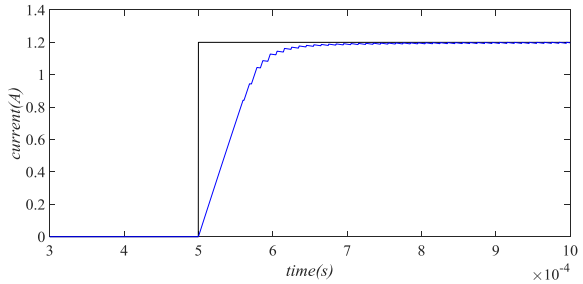

(c) Waveform under second set of PID parameters

Fig. 9. Waveforms of current tracking under three algorithms

From the above simulation results, it can be seen that when PID controller is used as the pre-controller, there is a conflict between tracking speed and overshoot, and it is difficult to find the optimal control parameter. With the one-cycle algorithm, the fastest tracking speed can be achieved without overshoot.

V. CONCLUSIONS

In this paper, a novel SVPWM control strategy for switching power amplifier is designed based on the main circuit

topology of two-phase three-leg switching power amplifier. One-cycle controller is used as the pre-controller for SVPWM, and the feasibility and superiority of this new control strategy are verified through simulation. This novel switching power amplifier can provide bidirectional current and can independently drive 2 DOF control coils. Besides, the output current has three states, with the characteristics of low current ripple with three-level control. At the same time, the number of switching tubes is reduced, thereby reducing the cost, the volume and switching loss of switching power amplifier. Compared with traditional SVPWM control strategy, this novel SVPWM control strategy has the advantages of high response speed, high tracking accuracy, and no overshoot. Therefore, the new algorithm has a better effect in the control of switching power amplifiers.

In the follow-up work, this novel SVPWM control algorithm will be experimentally verified, and the current closed loop experiment with inductor coil as the load will be performed and the magnetic bearing will be controlled.

VI. REFERENCES

[1] Schweitzer, G., and Maslen, E. H., "Magnetic bearings: theory, design, and application to rotating machinery," 2009.

[2] Lee, C., "Development of PWM Power Amplifier for Active Magnetic Bearings," vol. 4, pp. 3475-3478, 2004.

[3] Zhou, W., Wu, Z., Tang, J., and Liu, D., "A Novel Algorithm of SVPWM and the Study on the Essential Relationship Between SVPWM and SPWM," Proceedings of the CSEE, vol. 26, no. 2, pp. 133-137, 2006.

[4] Yang, G., Sun, L., Cui, N., and Liu, Y., "Study on method of the space vector PWM," Proceedings of the CSEE, vol. 21, no. 5, pp. 79-83, 2001.

[5] Suh, J., Choi, C., and Hyun D., "A new simplified space-vector PWM method for three-level inverters," vol. 16, no. 4, pp. 545-551, 2001.

[6] Tian, X., Fang, J., and Liu, G., "Magnetic bearing switching power amplifier based on SVPWM control," Systems Engineering and Electronics, vol. 30, no. 8, pp. 1598-1602, 2008.

[7] Zhou, L., Gong, W., and Su, X., "An Improved Switching Power Amplifier with One Cycle Control," *TRANSACTIONS OF CHINA ELECTROTECHNICAL SOCIETY*, vol. 19, no. 4, pp. 106-109, 2003.

[8] Jiang, T., Mao P., and Xie S., "Distortion Issue on Input Current of OCC-PFC Converter and Its Solution," Proceedings of the CSEE, vol. 31, no. 12, pp. 51-56, 2011.

[9] Wei, Z., Chen, X., Fan, Y., and Gong, C., "Study and Analysis of Neutral-point Potential and Control Methods for One-cycle Controlled Three-phase Three-level VIENNA Rectifiers," Proceedings of the CSEE, vol. 33, no. 15, pp. 29-37, 2013.

[10] Lei, T., Lin, H., and Zhang, X., "The Study of Operation for High Power Factor Rectifier in Unbalanced System Based on One-cycle Control," Proceedings of the CSEE, vol. 27, no. 36, pp. 109-114, 2007.

[11] Yang, D., Yang, M., and Ran, X., "One-Cycle Control for Double-Input Buck Converter," *TRANSACTIONS OF CHINA ELECTROTECHNICAL SOCIETY*, vol. 27, no. 1, pp. 162-171, 2012.

[12] Liu, C., Deng, Z., Cao, X., Li, K., and Zhou J., "An One-cycle Control Digital Control Strategy for Switching Power Amplifiers in Hybrid Magnetic Levitation Bearing Systems," Proceedings of the CSEE, vol. 35, no. 23, pp. 5899-5907, 2015.

[13] Liu, C., Deng, Z., Cao, X., Li, K., and Zhou J., "A Novel Control of Five-Phase Six-Leg Switching Power Amplifier in Magnetic Levitating Bearing System," *TRANSACTIONS OF CHINA ELECTROTECHNICAL SOCIETY*, vol. 31, no. 9, pp. 112-119, 2016.

[14] Zhou, J., Deng, Z., Li, K., He, J., "Digital One-cycle Control Algorithm with Compensation of Time Delay for Switching Power Amplifier in Magnetic Suspension Bearings," Transactions of China Electrotechnical Society, 2017.

[15] Wang, Y., Du, J., Tao, W., and Chen, Y., "Study of SVPWM based on DSP," Electric Machines and Control, vol. 4, no. 2, pp. 98-105, 2000.

[16] Li, B., "Research of the Integration Technology in the Magnetic Bearing System", 2003.

[17] Li, X., "The Study of Novel Switching Power Amplifiers for Magnetic Bearings," 2005.